PFC/RR-82-12

DOE/ET-51013-43
UC20

Heating Rates and Absorption Coefficients for Electron Cyclotron Heating in the Constance 2 Mirror Experiment

by

Michael E. Mauel

April, 1982

Plasma Fusion Center
Research Laboratory of Electronics
Massachusetts Institute of Technology
Cambridge, MA 02139

THIS WORK WAS SUPPORTED BY DOE CONTRACT NO. DE-AC02-78ET-51013.

PFC-RR-82/12

DOE/ET-51013- 43
UC-20

Heating Rates and Absorption Coefficients for Electron Cyclotron Heating in the Constance 2 Mirror Experiment.

by

Michael E. Mauel

April, 1982
Plasma Fusion Center
Research Laboratory of Electronics
Massachusetts Institute of Technology

This report presents and discusses the calculation of heating rates and absorption coefficients of electron cyclotron waves in a mirror. In particular, the scaling of the heating rates with resonant zone location and plasma density are calculated since this scaling can be compared with the measurements made on the Constance 2 mirror experiment. Both geometric and Doppler broadening are included by making the substitution $\Delta\omega^2 \equiv (\omega N_{\|}\beta)^2 \rightarrow (\omega N_{\|}\beta)^2 + \left\langle \tau_{eff}^{-2} \right\rangle$, where $\langle \tau_{eff} \rangle$ is the average transit time of electrons through the resonance layer. The energy transfer between the waves and the electrons are calculated with the same bounce-averaged resonance function used in a Fokker-Plank code[1,2]. A simple scaling law for the heating rate is shown to be consistent with the Fokker-Plank results for Maxwellian electrons.

This report estimates the absorption of electron cyclotron waves in the Constance 2 mirror experiment. In particular, the scaling of the heating rate with resonant zone location and plasma density are calculated since this can help interpret the experimental results. Mauel[1,2] are companion papers to this report and describe with more detail the general theory of electron cyclotron heating in mirrors and the Fokker-Plank code used to model the experimental results. The theory is based on the works of Berk[3] and Bernstein and Friedland[4]. The report is divided into three sections. The first section introduces the notation and approximations by describing briefly the dispersion tensor and resonance function (see, also, Mauel[1]). The second section describes the expressions for the heating rates and absorption coefficients consistent with a WKB approximation to the actual wave propagation[5]. The final section presents and discusses the results in light of sample experimental data.

1. The Dispersion Relation and Resonance Function .

By expanding the electric field, $\overline{\mathrm{E}}_k(t')$, about the local guiding center coordinates and the current time, and by integrating along the bouncing, particle orbits, a WKB formalism of the propagation and absorption of electromagnetic waves in a mirror results[1]. The approximate, local relationship between the index of refraction, N, the plasma and cyclotron frequencies, ω_{pe}, ω_{ce}, the electron distribution, $F_0(\mu, E, \overline{X})$, and the wave frequency, ω is given by the well-known dispersion tensor, or

$$\frac{\mathrm{D}^{ij^*}}{\omega} \approx (1 - N^2)\delta^{ij} + N^i N^{j^*} - i\frac{\omega_{pe}^2}{\omega}\sum_n \sum_{\pm} \int \frac{dE d\mu B}{|v_{\|}|} v^i v^{j^*} J_n^2(k_\perp \rho)\, \Omega_n^{-1} \frac{\partial F_0}{\partial \chi} \qquad (1)$$

where the $(r, l, \|)$ basis is used. As explained in Mauel[1], $v^i v^{j^*}$ contain operators on the order of the bessel function, but for our purposes only the right-handed velocities will be important so that $v^r v^{r^*}$ becomes $B\mu$

and the order of the bessel function is reduced from n to $n-1$. Other larmor radius effects are ignored since, for Constance 2, $k_\perp \rho = N_\perp \beta \ll 1$. The derivative, $\partial/\partial\chi$, is the gradient along the wave-induced electron diffusion path, or

$$\frac{\partial}{\partial \chi} = \frac{1}{B}\frac{\partial}{\partial \mu} + \frac{\partial}{\partial E} - \frac{N_{||}\beta_{||}}{B}\frac{\partial}{\partial \mu} \tag{2}$$

where the drift-dependent, radial transport term is small and can be ignored. When evaluated at resonance, $\nu_n \equiv \omega - n\omega_c - k_{||}v_{||} = 0$, and Equation 2 becomes

$$\left.\frac{\partial}{\partial \chi}\right|_{res} = \frac{1}{B_{res}}\frac{\partial}{\partial \mu} + \frac{\partial}{\partial E} \tag{3}$$

where $\omega = n\omega_{ce,res}$. Finally, note that F_0 is normalized to unit density.

The term Ω_n^{-1} is the local resonance function, or

$$\Omega_n^{-1} = \int_{-\infty}^{0} dt' e^{-i\int_0^{t'} \nu_n(t'')dt''} \tag{4}$$

It is this term which contains the details of the wave-particle interaction.

For a homogeneous plasma (*ie.* when geometric broadening can be ignored), $\nu(t)$ is constant, and Ω_n^{-1} becomes

$$\Omega_n^{-1} \approx \mathsf{P}\frac{i}{\nu_n} + \pi\delta(\nu_n) \tag{5}$$

where P refers to the principle value and $\delta(x)$ is the Dirac delta function. Those electrons exactly in resonance are purely resistive, and the remaining particles are purely reactive. For Maxwellian electrons, Equations 1 and 5 give the right-handed permittivity as $\epsilon^{rr^*} = 1 + \chi^{rr^*}$, and

$$\chi^{rr^*} \approx X\frac{\omega}{\Delta\omega}Z\left(\frac{\omega - \omega_{ce}}{\Delta\omega}\right) \tag{6}$$

Here, $X = \omega_{pe}^2/\omega^2$, $\beta = v_{the}/c$, $\Delta\omega = \omega N_{||}\beta$, and Z is the plasma dispersion function. The term $\Delta\omega$ represents the Doppler broadening of the (infinite-medium) cyclotron resonance. For a plasma in an inhomogeneous magnetic field, Doppler broadening shifts the resonance along a field line by an amount $\delta s \approx -\omega N_{||}\beta/n(\hat{\mathbf{b}}\cdot\nabla)\omega_{ce}$.

When $\nu(t)$ is not constant (*ie.* for the heating of mirror-confined particles considered in this report), the resonance function can be approximated by the local derivatives of ν_n. In this case, the particles are resonant at specific times during their orbits and exchange energy with the wave during a finite time, τ_{eff}. In general, each particle contributes both a reactive and resistive part to the permittivity. In this report, this effect is referred to as "geometric broadening" and is proportional to the inverse transit time, τ_{eff}^{-1}.

Mathematically, ν_n in Equation 4 is expanded backwards in time along a particle's bounce-orbit. The contribution to the integral for times in the distant past can be safely ignored provided that the electric field is large enough so that the electron motion is not superadiabatic. In this case, the wave and particle are decorrelated during each resonance passing. As in Mauel[1], when $\nu_n' \neq 0$, the integral in Equation 4 becomes

$$\begin{aligned}\Omega_n^{-1} &\approx \int_{-\infty}^{0} dt' e^{-i(\nu_n t' + \tau_{eff}^{-2} t'^2)} \\ &\approx \frac{1}{2i}\tau_{eff} e^{-i\pi/4} Z\left(\frac{1}{2}\nu_n \tau_{eff} e^{-i\pi/4}\right)\end{aligned} \tag{7}$$

where $\tau_{eff}^{-2} = \nu_n'/2$ and $Z(z)$ is the plasma dispersion function. On the other hand, as $\nu_n' \to 0$, the next order expansion gives

$$\begin{aligned}\Omega_n^{-1} &\approx \int_{-\infty}^{0} dt' e^{-i(\nu_n t' + \tau^{-3} t'^3/3)} \\ &\approx \pi|\tau_{eff}| Ai(\nu_n \tau_{eff}) + i\pi\tau_{eff} Gi(\nu_n \tau_{eff})\end{aligned} \tag{8}$$

where, in this case, $\tau_{eff}^{-3} = \nu_n''/2$. When $\nu_n = 0$, $\nu_n' \neq 0$, $\Omega_n^{-1} = e^{-i\pi/4}\sqrt{\pi}\tau_{eff}/2$, and when $\nu_n' \approx 0$, $\Omega_n^{-1} = 0.355\pi(|\tau_{eff}| + i\tau_{eff}/\sqrt{3})$. For the first case (Equation 7), the integral over $\pm v_\parallel$ cancels the reactive part at $\omega = \omega_{ce}$ since ν_n' changes sign. However, due to the particles which turn at within the absorption layer (*ie.* when $\nu' \to 0$), the total integral of the reactive part remains finite and, instead, vanishes slightly off resonance.

The appropriate local expressions for ν' and ν'' in these equations are given by the following formulas

$$\nu_n = \omega - n\omega_c - k_\parallel v_\parallel \tag{9}$$

$$\nu_n' = -nv_\parallel(\hat{b}\cdot\nabla)w_c + k_\parallel\mu(\hat{b}\cdot\nabla)B \tag{10}$$

$$\nu_n'' = n\frac{\omega_c}{B}\left\{\mu(\hat{b}\cdot\nabla B)^2 - v_\parallel^2(\hat{b}\cdot\nabla)^2 B\right\} + k_\parallel v_\parallel \mu(\hat{b}\cdot\nabla)^2 B \tag{11}$$

Note that the local "bouncing" resonance function is determined by the constants of the motion, the local magnetic field strength, and the first and second derivatives of $|B|$ along the field lines. For deeply trapped particles, the bounce frequency is given by $\omega_{ce}\omega_B^2 = \mu(\mathfrak{b}\cdot\nabla)^2\omega_{ce}$ or $\omega_B \sim v_\perp/L_B$. Finally, note that Equations 7 through 11 still include the Doppler shift while simply "smearing" the delta-function interaction of Equation 5 over the time τ_{eff}.

In order to incorporate Equations 7 and 8 into a more useful form, an *ad hoc* approximation is made to eliminate the need to numerically integrate the resonance function when evaluating $\chi_R^{rr^*}$. The broadening term in the infinite medium result is changed by the simple substitution

$$\Delta\omega^2 = (\omega N_{||}\beta)^2 \rightarrow (\omega N_{||}\beta)^2 + \left\langle \tau_{eff}^{-2} \right\rangle \tag{12}$$

where $\langle\tau_{eff}\rangle$ includes the geometric part with the term proportional to $k_{||}$ removed. $\Delta\omega$ remains the breadth of the integral of the resonance function and is made equal to the geometric mean of the breadth of Doppler term with an instantaneous interaction and the geometric breadth without Doppler broadening. Assuming Maxwellian electrons, $\langle v_{||}\rangle \sim \langle v_\perp\rangle \sim c\beta$, and the expressions for $\langle\tau_{eff}\rangle$ become

$$\left\langle \tau_{eff}^{-2} \right\rangle \approx \frac{c\beta}{2}\,\mathfrak{b}\cdot\nabla\,\omega_{ce} \tag{13}$$

when $(\mathfrak{b}\cdot\nabla\,\omega_{ce})^3 > 2c\beta\,[(\mathfrak{b}\cdot\nabla)^2\omega_{ce}]^2$ and

$$\left\langle \tau_{eff}^{-2} \right\rangle \approx \left[\frac{c^2\beta^2}{2}(\mathfrak{b}\cdot\nabla)^2\,\omega_{ce}\right]^{2/3} \tag{14}$$

for the opposite inequality. The inequality states that the second-order expansion is used provided $\langle\tau_{eff}\rangle$ never exceeds the bound set by the third-order expansion. The above approximation actually serves two purposes since both an analytic expression for the geometric effect is obtained and, at the same time, the oscillatory part of the resonance function (which occurs after a particle's passage through the absorption layer) is by-passed, avoiding the development of more detailed approximations necessary to deal with the de-correlation of the wave and particle with finite fields.

From Equation 12, geometric broadening becomes important when $\left\langle \tau_{eff}^{-1} \right\rangle > \omega N_{||}\beta$ which is equivalent to the condition that the effective length of the energy exchange $\langle v_{||}\tau_{eff}\rangle$ is larger than the mean Doppler shift. Thus the condition for geometric broadening to dominate is when $N_{||}^2 < (1/2\beta)\,(c\mathfrak{b}\cdot\nabla\,\omega_{ce})$. For the Constance 2 experiment, with $\beta \sim 0.01$, the geometric effect makes only a small change in the polarization and damping predicted by the infinite medium theory whenever $N_{||} > 1$. However, for

propagation within 10 or 15 degrees of the normal to the magnetic field, geometric broadening significantly increases the strength of the right-handed polarization and, therefore, the absorption coefficients. Note that, in addition to Doppler broadening, the relativistic mass shift will broaden the resonance by an amount $\delta s_{rel} \approx \beta\omega_{ce}/\hat{\mathbf{b}}\cdot\nabla\,\omega_{ce}$. Therefore, using the same arguments as above, when $N_{\|} \rightarrow 0$, geometric broadening is significantly increases the absorption whenever $\beta^2 < (2c/\omega^2)\hat{\mathbf{b}}\cdot\nabla\,\omega_{ce}$, or, for Constance 2, whenever $T_e \lesssim 30kev$.

In addition to the local resonance function, the integral of Ω_n^{-1} along the particle's orbit, or the bounce-average, is used to calculate the Fokker-Plank diffusion coefficient and the total, single-pass absorption coefficient. These are derived in Mauel[1] and are given as

$$Re\{\overline{\Omega_n^{-1}}\} = \frac{1}{4}\omega_B\tau_{eff}^2 \qquad (\text{where } \tau_{eff}^{-2} = \nu_n'/2) \tag{15}$$

$$Re\{\overline{\Omega_n^{-1}}\} = 2\pi\omega_B\tau_{eff}^2 Ai^2(\nu_n\tau_{eff}) \qquad (\text{where } \tau_{eff}^{-3} = \nu_n''/2) \tag{16}$$

τ_{eff} is defined as before. Only the real part is needed, representing the irreversible, resonant wave-particle energy exchange. Note that Equation 15 can be checked by bounce-averaging $\pi\delta(\nu_n)$ in Equation 5. However, to obtain Equation 16, the full evaluation of the phase integral of Equation 4 is necessary as was first done by Berk[3].

2. Physical Optics .

The equation for the wave energy flow results when terms of order $1/kL$ are retained. This gives the physical optics equation

$$\nabla\cdot(\mathbf{v}_g^i W_k^i) + \frac{\partial W_k^i}{\partial t} + 2\mathbf{k}_I\cdot\mathbf{v}_g^i W_k^i = 0 \tag{17}$$

where $\mathbf{v}_g^i$ is the group velocity for the ith mode, or

$$\mathbf{v}_g^i = -\frac{\partial D_R^i}{\partial \mathbf{k}}\left(\frac{\partial D_R^i}{\partial \omega}\right)^{-1} \tag{18}$$

W_k^i is the total wave energy, or

$$W_k^i = \frac{1}{8\pi}|E^i|^2\frac{\partial D_R^i}{\partial \omega} \tag{19}$$

$\mathbf{k}_I = -D_I^i \left(\frac{\partial D_R^i}{\partial \mathbf{k}} \right)^{-1}$ is the local damping rate, and the "modes" are to be considered to be defined by the local dispersion tensor, which is an eigenvalue equation for the index of refraction and the polarization. $D^i = D_R^i + iD_I^i$ is the complex diagonal element of $\mathbf{D}^{ij^*}$ in the basis of the mode polarizations.

Using the bounce-averaged quasilinear equation[1], the heating rate is given by

$$\frac{\partial(nE)}{\partial t} = \frac{1}{4\pi} \sum_{res} \overline{\mathbf{D}}_I^{ij^*} |\overline{E}^{i^*} \overline{E}^j|_k \tag{20}$$

where the "bar" over $\mathbf{D}_I^{ij^*}$ signifies that the bounce-averaged resonance function is to be used. Using Equations 18 and 19, Equation 20 can be rewritten into a more useful form by defining the heating rate per unit input power flux

$$\frac{1}{(v_g W_k)_{res}} \frac{\partial(nE)}{\partial t} = 2 \sum_{res} \overline{\mathbf{D}}_I^{rr^*} \mathcal{E}_{res} \tag{21}$$

where $\mathcal{E}_{res}$ is the resonant electric field energy per input power flux, or

$$\mathcal{E}_{res} \equiv - \frac{|\overline{E}_r|^2}{|\overline{E}^{i^*} \overline{E}^j|_k \left| \frac{\partial \mathbf{D}_H^{ij^*}}{\partial \mathbf{k}} \right|} \tag{22}$$

The heating rate per input power flux has the dimensions of $area \cdot volumn^{-1}$ or $length^{-1}$, and the dimensions of $\mathcal{E}_{res}$ is $speed^{-1}$. For a right-handed wave in a vacuum, $\mathcal{E} = 1/2c$. For a cold plasma, $\mathcal{E}_{res} \rightarrow 0$ since the electrons effectively "short-out" the resonant polarization. For a thermal plasma, with finite $\Delta\omega$, $\mathcal{E}_{res}$ remains finite. In addition to the heating rate, $\mathcal{E}_{res}$ is used to give the local damping rate

$$k_I = \mathbf{D}_I^{rr} \mathcal{E}_{res} \tag{23}$$

Finally, another way to utilize the bounce-averaged resonance function is to calculate the single-pass absorption coefficient. This is given by the integral of $\mathbf{k}_I$ along a ray trajectory which passes through a resonance, or

$$\langle 2k_I L_{res} \rangle = 2 \oint_{ray} \mathbf{k}_I \cdot \mathbf{v}_g d\tau \tag{24}$$

As explained in Friedland and Porkolab[6], the absorption layer, L_{res}, is often short compared to the scale-lengths of changes in the dispersion tensor and the ray path. In these cases, the slowly varying quantities in the integral above can be approximated by their values at resonance. Then, using geometry to relate the integral along the ray trajectory to an integral along the magnetic field line,

$$\langle 2k_I L_{res}\rangle = 2\frac{cos\phi}{\cos(\phi-\xi)}\oint \mathfrak{b}\cdot \mathrm{k}_I\, ds \tag{25}$$

where $cos\phi \sim \nabla|\mathrm{B}|\cdot\mathrm{B}$ and $cos\xi \sim \mathrm{v}_g\cdot\mathrm{B}$. The value of N, θ, ϕ, and ξ can all be found in the appropriate geometry by using a ray tracing code. Note that when $\phi-\xi\rightarrow\pi/2$, the ray is no longer "crossing"the resonance zone and the approximation breaks down. The integral over ds becomes a bounce average by the transformation

$$\oint ds \rightarrow \oint v_{\|}\tau_B\frac{d\psi}{2\pi} \tag{26}$$

where τ_B is the bounce period. Then,

$$\langle 2k_I L_{res}\rangle \approx 2\omega_{pe}^2\frac{\cos\phi}{\cos(\phi-\xi)}\,\overline{\mathcal{E}}_{res}\int d^3v\, v_{\|}\tau_B Re\{\overline{\Omega_n^{-1}}\}B\mu\frac{\partial F_0}{\partial\chi} \tag{27}$$

For simplicity, the factor $v_{\|}\tau_B$ can be replaced by multiplying $\overline{\mathsf{D}}^{rr^*}$ by $\langle v_{\|}\tau_B\rangle \sim 2\pi L_B$, then the first-pass absorption is related to the heating rate per input power flux by the formula

$$\langle 2k_I L_{res}\rangle \approx \langle v_{\|}\tau_B\rangle\frac{\cos\phi}{\cos(\phi-\xi)}\,\frac{1}{(v_g W_k)_{res}}\frac{\partial(nE)}{\partial t} \tag{28}$$

which is just a statement of conservation of energy. Furthermore, as shown in the next section, a good approximation to $Re\{\overline{\Omega_n^{-1}}\}$ is $2\pi\left\langle\omega_B\tau_{eff}^2\right\rangle$. Then, Equation 28 becomes

$$\langle 2k_I L_{res}\rangle \approx 8\pi^2\left\langle v_{\|}\tau_{eff}^2\right\rangle\omega_{pe}^2\,\mathcal{E}_{res}\frac{cos\phi}{cos(\phi-\xi)} \tag{29}$$

where $\left\langle v_{\|}\tau_{eff}^2\right\rangle \sim 1/\mathfrak{b}\cdot\nabla\omega_{ce}$ when Equation 13 is valid.

It should also be mentioned that when the heating rate per input power flux is much greater than one, the absorption is strong enough that the wave is damped well before the turning-point resonance. If

the propagation angle is small, then only those particles which have their resonances Doppler shifted in the direction of the incoming wave absorb energy. In other words, the hot, passing particles get hotter while the cooler, turning particles absorb little. If the propagation is nearly perpendicular to B, then the resonance width is determined by geometric broadening which scales only as the square-root of velocity and tends to reduce "hot-particle, Doppler shielding". Nevertheless, in either case, when there is strong damping, both the WKB formalism and the velocity-space integral over the bounce-averaged resonance function found in $\overline{D}_J^{rr^*}$ are not valid.

3. Results .

Figures 1 and 2 show $\mathcal{E}_{res}$ and $X\mathcal{E}_{res}$ as a function of $X = \omega_{pe}^2/\omega^2$ for several values of the propagation angle, $\theta = cos^{-1}(\hat{\mathbf{k}} \cdot \hat{\mathbf{b}})$. $\mathcal{E}_{res}$ is the right-handed field energy per input power flux at resonance, and $X\mathcal{E}_{res}$ scales as the heating rate and first-pass absorption. The two limiting cases of parallel and perpendicular propagation are the well-known whistler and extra-ordinary modes. (See for example Akhiezer, *et. al.*[7], Eldridge, *et. al.*[8], and Fidone, *et. al.*[9].) For nearly parallel propagation, nearly all of the electric field energy is right-handed and $\mathcal{E}_{res}$ is nearly independent of X. On the other hand, for perpendicular propagation, the electrons "short-out" the resonant field. In this case, $\overline{E}_r \sim 1/\chi^{rr^*} \sim \Delta\omega/X$, giving $\mathcal{E}_{res} \sim (\Delta\omega/X)^2$. Note, that without geometric broadening $\mathcal{E}_{res} \sim N_{||}^2\beta^2$ which vanishes as $N_{||} \to 0$.

Knowing $\mathcal{E}_{res}$, the heating rate (Equation 21) can be calculated by numerically integrating the bounce-averaged resonance function to obtain $\overline{D}_J^{rr^*}$. This is shown in Figure 3 as a function of the midplane field, ω_{c0}. (The RF frequency is fixed so that as the field is raised, the resonance zones move toward the midplane from the mirror peaks.) The field is assumed parabolic, $L_B = 33cm$, and the distribution Maxwellian, $T_e = 50ev$. The density is made to decay axially as a Gaussian with a mean of $L_p = 15cm$, and the peak value of X is 0.92. Also plotted is the useful approximation

$$\overline{D}_J^{rr^*} \approx 2\pi\omega_{pe}^2\left\langle \omega_B\tau_{eff}^2 \right\rangle \tag{30}$$

where the factor of 2π was added to fix the numerical results. Notice that $\overline{D}_J^{rr^*}$ is linearly dependent on n_e while (at this range of temperatures) nearly independent of $N_{||}$ and T_e. On the other hand, the heating rate is strongly dependent on these parameters through $\mathcal{E}_{res}$. To illustrate this, Figure 4 graphs the heating rate for four propagation angles, θ =0.2, 0.6, 1.0, and 1.4 for four values of the peak X =0.37, 0.55, 0.73, and 0.92. Note, that for perpendicular propagation, the heating rate is either independent or decreasing function of ω/ω_{c0} while for small θ, $X\mathcal{E}_{res}$ is nearly independent of X and the heating rate reflects the increase in $\left\langle \tau_{eff}^2 \right\rangle$ as $\omega/\omega_{c0} \to 1$.

Another, more graphic way to illustrate the scaling of the heating rate with density and resonant zone

location is shown in Figures 5 and 6. Figure 5b show contour plots of $\omega_{pe}^2\left\langle \omega_B \tau_{eff}^2 \right\rangle \mathcal{E}_{res}$ for a model of the magnetic geometry used to calculate the ray trajectories[10] in Constance 2 (shown in Figure 5a). The radial scale of the plasma density at the midplane is about $1.5cm$, and the length on axis is $15cm$. X at the origin is 0.92, which is typical for the Constance 2 experiment. The height of the contours approximate the heating rate if the magnetic field was adjusted to be resonant at that location (ω is constant) and if the propagation angle was fixed by that indicated in each figure ($\theta = 0.2, 0.6, 1.0$, and 1.4). Figure 6 shows the heating rate as a function of radius at the midplane for these same four cases to indicate the larger absorption at the edge of the plasma due to the reduction of $\mathcal{E}_{res}$ at high densities.

In the Constance 2 experiment, the scaling of the heating rate and the radial profile of the heating can be estimated with diamagnetism measurements. Although these measurements cannot prove or disprove the theoretical calculations reported here, they are the only measurements available which can be compared with the numerical results. A complete description of the goals and construction of the Constance 2 experiment will not be given here, but details can be found in either *Constance 2: Progress and Plans*[11] or a copy of "Electron Cyclotron Heating in the Constance 2 Mirror Experiment"[12]. For the sample data shown here, the only special information needed is that the experiment is divided into two parts. In the first part, the propagation angle and input power flux at each resonance region are not known since the microwaves bounce within the vacuum chamber and through the plasma several times before being absorbed. This is evidenced by the observed equal heating efficiencies when the launch geometry was changed, and the constant ratio of local RF measurements at different positions in the chamber. In this case, the power should be absorbed by the modes with the highest first-pass absorption (*ie.* small propagation angles), and at those regions with the highest heating rates, which is at the edge, as shown in Figures 5 and 6. All of the following data are samples from this part of the experiment. In the second part (not yet completed), absorbing liners will be placed within the chamber which should reduce the intensity of the power radiated back from the walls.

Figure 7 shows a sample of the scaling of the initial rate of rise of diamagnetism with midplane field for two values of peak density $X \approx 1.2$ and 0.25. The diamagnetism is measured with a large loop encircling the plasma. (The magnetic flux, $\delta\Phi$, linking the loop is related to the product of the density and temperature through $\delta\Phi B_0 \sim \pi R_p^2 \delta\langle nT_\perp \rangle$.) The rate of rise of diamagnetism scales as the heating rate provided that the plasma geometry does not change. However, as the midplane field is lowered, the axial and radial location of the heating zone moves away from the origin which may modifies the coupling of the heated plasma to the loop. Nevertheless, since the loop's diameter is 4 to 10 times larger than the plasma and is positioned axially almost midway between the midplane and the position of the resonant zone at the lowest field tested, these coupling variations should be minimized. If the possible changes in the coupling are assumed small, then Figure 7 shows an insignificant difference between the high and low density cases and shows a peak in the heating rate when the midplane field is resonant at the midplane. Since the most strongly absorbing regions of the mirror are at the edge, the increase in density is expected to push the heating further away from axis but not necessarily modify the total heating rate. The peaking of the heating rate when $\omega = \omega_{c0}$ would be

expected from the increase in $\left\langle \omega_{pe}\tau_{eff}^2 \right\rangle$ and scaling of the highly absorbent, small θ modes shown in Figure 4.

To further demonstrate edge heating, Figure 8 shows the radial profile of the plasma density (before and after ECRH) as measured with a Langmuir probe and the radial profile of the change in the axial magnetic field due to the heated electrons. The flux profile was measured with a small, movable magnetic probe. The increase in plasma density is due to the ionization of the neutral gas around the plasma. The "paramagnetic" signal on the magnetic probe is the return flux of the increased diamagnetism of the electrons. The radial position where the flux does not change is the effective radius of the heated plasma which is significantly larger than the radius of the density. In fact, floating probe signals show large negative potentials (indicative of heating) out past $10cm$ from the axis.

Acknowledgment.

The author would like to acknowledge several enlightening conversations concerning this work with his colleague, R. Garner, and thank R. E. Klinkowstein for designing and building the magnetic probe. The numerical work of this report was obtained with use of the Macsyma Consortium computer at M.I.T.. This work was supported by D. C. E. Contract No. DE-AC-78ET-51013.

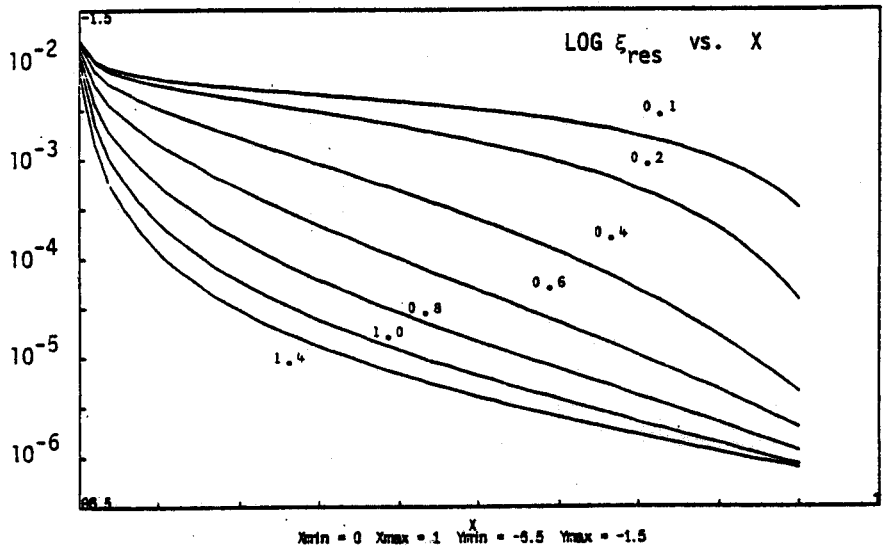

Figure 1. $\mathcal{E}_{res}$ as a function of $X = \omega_{pe}^2/\omega^2$ for $\theta \equiv cos^{-1}(\hat{\mathbf{k}} \cdot \hat{\mathbf{b}}) =$ 0.1, 0.2, 0.4, 0.6, 0.8, 1.0, and 1.4. Note, the nearly $1/X^2$ dependence of $\mathcal{E}_{res} \sim 1/|\chi^{rr^*}|^2$ for small θ.

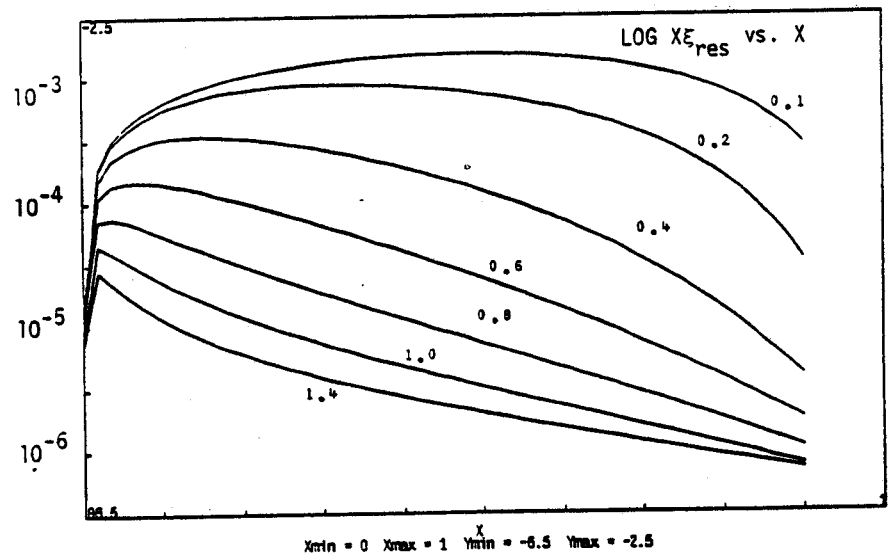

Figure 2. The product $X\,\mathcal{E}_{res}$ verses X which is scales as the heating rate and first-pass absorption. Same parameters as in Figure 1.

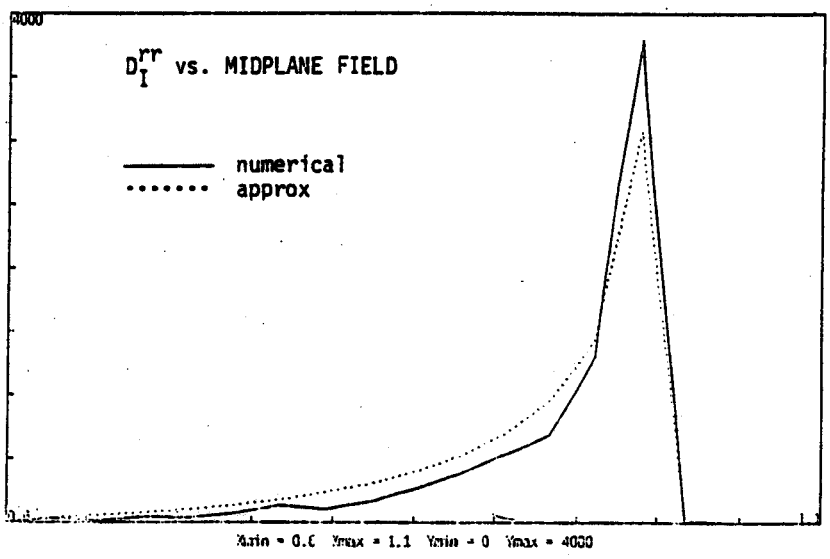

Figure 3. $\overline{D}_I^{rr}$ and the approximate heating rate $2\pi\omega_{pe}^2\left\langle \omega_B \tau_{eff}^2 \right\rangle \mathcal{E}_{res}$ for the same parameters as Figure 3.

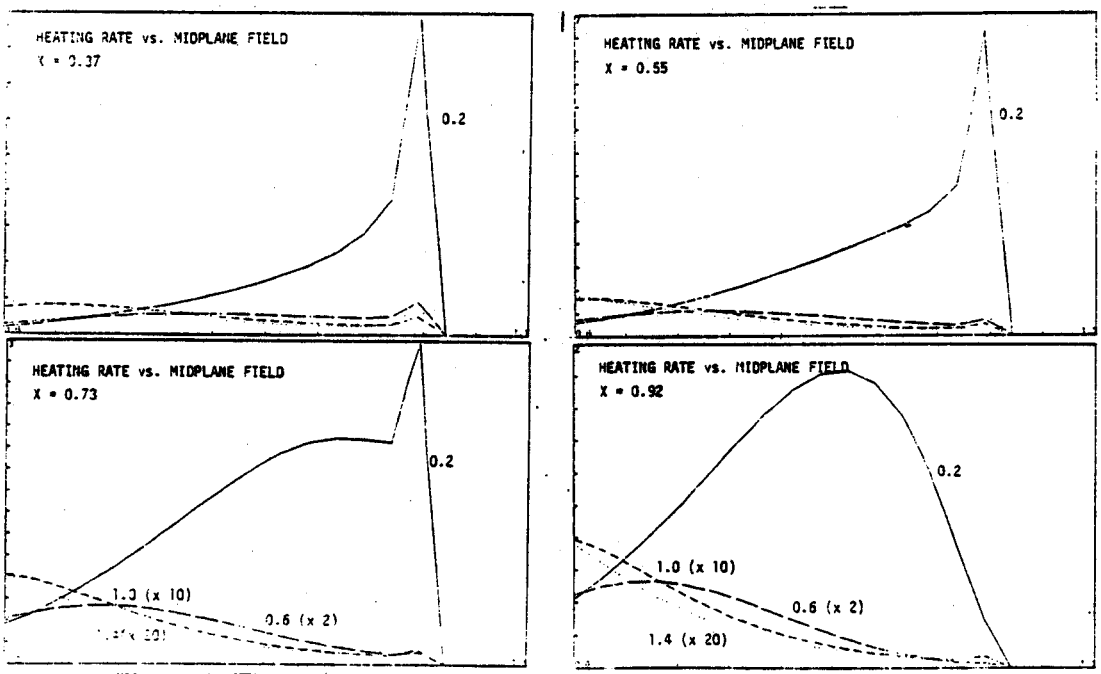

Figure 4. The approximate heating rates for $\theta = 0.2, 0.6, 1.0,$ or 1.4. The axial density scale length is $L_p \sim 15cm$.

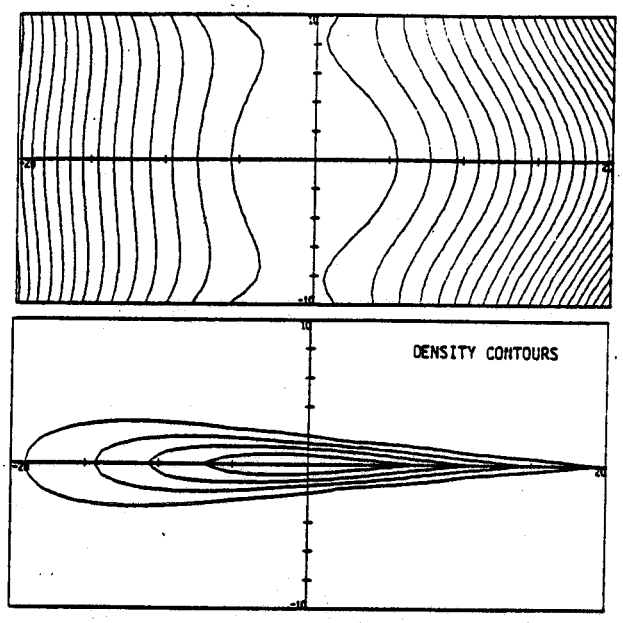

Figure 5a. Contour plots of the density and magnetic field contours which model the Constance 2 plasma.

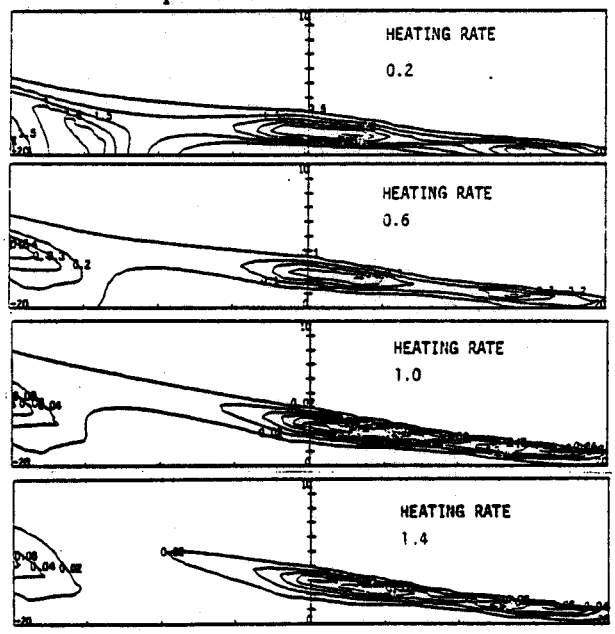

Figure 5b. The corresponding contours of $\omega_{pe}^2\left\langle \omega_B \tau_{eff}^2 \right\rangle \mathcal{S}_{res}$ at each point assuming that the propagation angle was fixed at either $\theta = 0.2, 0.6, 1.0,$ or 1.4. The contour height is proportional to the heating rate at that coordinate if the field was adjusted to give resonance. Notice the that the peak heating is at the edge of the plasma.

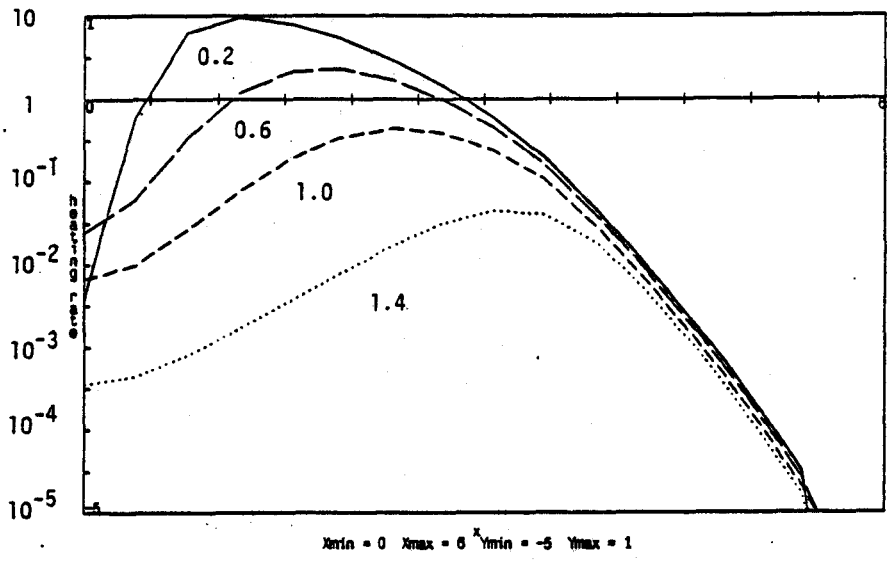

Figure 6. The cross-section of the heating rate shown in Figure 6b at the midplane verses radius.

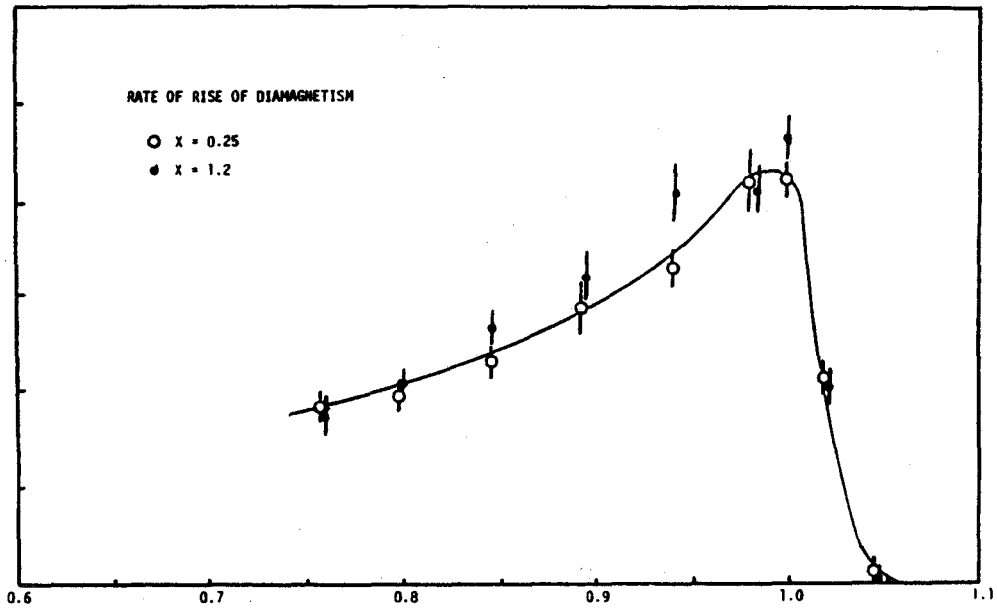

Figure 7. The scaling of the initial rate of rise of diamagnetism as the midplane field is changed. The open circles are for a peak $X \sim 0.25$ and the closed circles are for $X \sim 1.2$. Ignoring changes in the plasma geometry, this is a measurement of the heating rate.

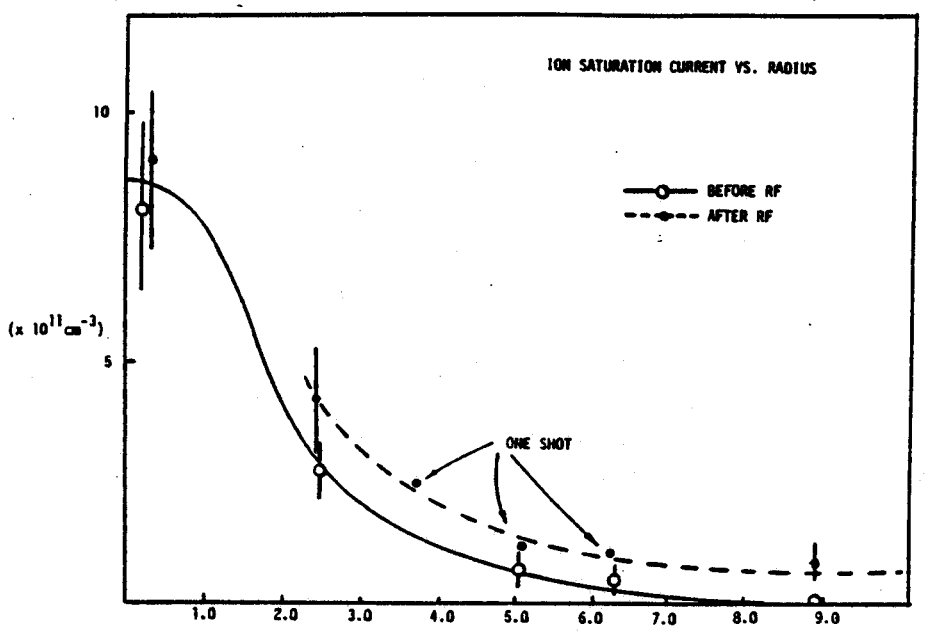

Figure 8a. The plasma density profile measured with a Langmuir probe. The line density measured with a 60GHz interferometer gives the vertical scale. Data taken before and after heating. The increase in density is due to ionization.

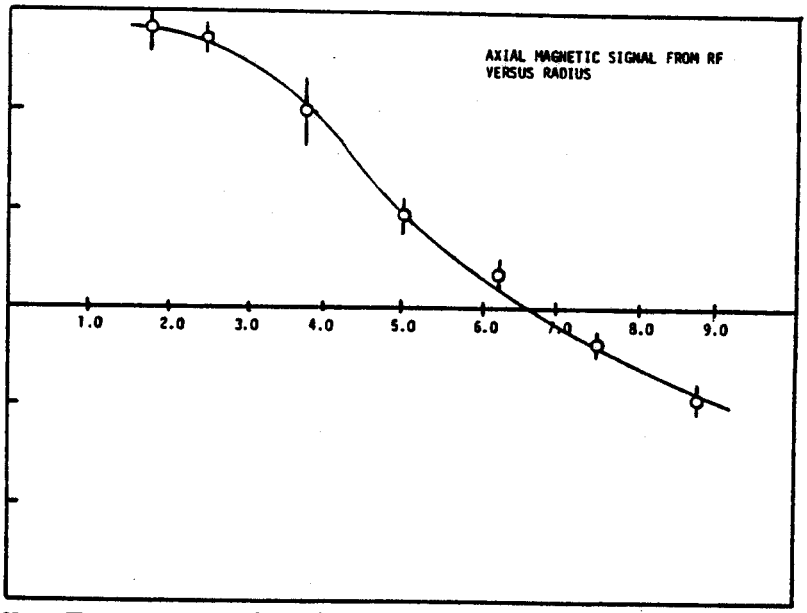

Figure 8b. The radial profile of the change in axial magnetic field due to the heated electrons. The midplane field was adjusted so that the resonance zone was $\sim 5cm$ of the midplane with $\omega/\omega_{c0} = 1.02$. Notice that the radial width of ΔnT from the ECRH is wider than the density profile.

References

1. Mauel, M. E., *Theory of Electron Cyclotron Heating in the Constance II Experiment*, PFC-RR-81/2, Massachusetts Institute of Technology, (1981).

2. Mauel, M. E., *Description of the Fokker-Plank Code Used to Model ECRH of the Constance 2 Plasma*, PFC-RR-82/2, Massachusetts Institute of Technology, (1982).

3. Berk, H. L., "Derivation of the Quasilinear Equation in a Magnetic Field," *J. Plasma Physics*. **20**, (1978), 205-219.

4. Bernstein, I. B., and D. C. Baxter, "Relativistic Theory of Electron Cyclotron Heating," *Physics of Fluids*. **24**, (1981), 108-126.

5. Bernstein, I. B., "Geometric Optics in Space- and Time-Varying Plasmas," *Physics of Fluids*. **18**,, 320-324.

6. Friedland, L. and M Porkolab, *On the Electron-Cyclotron Resonance Heating in Plasmas with arbitrary Stratification of the Magnetic Field*, PFC-JA-80/21, Massachusetts Institute of Technology, (1980).

7. Akhiezer, A. I., *et. al.*, *Plasma Electrodynamics*. Vol. 1, Pergamon, (1975).

8. Eldridge, O., *et. al.*, *Electron Cyclotron Heating in Tokamaks*. ORNL/TM-6052, Oak Ridge National Laboratory, (1977).

9. Fidone, I., *et. al.*, "Wave Absorption near the Electron Cyclotron Frequency," *Physics of Fluids*. **21**, (1978), 645-652.

10. Garner, R. and M. Mauel, "Ray Tracing in the Constance 2 Mirror Experiment," *Bull. Amer. Phys. Soc.*. **26**, (1981), 893.

11. Klinkowstein, R. E., *et. al.*, *Constance 2: Progress and Plans*, PFC-RR-81/3, MIT, (1981).

12. Mauel, M. E., *et. al.*, "Electron Cyclotron Heating in the Constance 2 Experiment," *Bull. Amer. Phys. Soc.*. **26**, (1981), 893.

PFC BASE LIST

INTERNAL MAILINGS (MIT)

G. Bekefi
36-213

A. Bers
38-260

D. Cohn
NW16-250

B. Coppi
26-201

R.C. Davidson
NW16-202

T. Dupree
38-172

S. Foner
NW14-3117

J. Freidberg
38-160

A. Gondhalekar
NW16-278

M.O. Hoenig
NW16-176

M. Kazimi
NW12-209

L. Lidsky
38-174

E. Marmar
NW16-280

J. McCune
31-265

J. Meyer
24-208

D.B. Montgomery
NW16-140

J. Moses
NE43-514

D. Pappas
NW16-272

R.R. Parker
NW16-288

N.T. Pierce
NW16-186

P. Politzer
NW16-286

M. Porkolab
36-293

H. Praddaude
NW14-3101

D. Rose
24-210

J.C. Rose
NW16-189

R.M. Rose
4-132

B.B. Schwartz
NW14-5121

R.F. Post
NW21-203

L.D. Smullin
38-294

R. Temkin
NW16-254

N. Todreas
NW13-202

J.E.C. Williams
NW14-3210

P. Wolff
36-419

T.-F. Yang
NW16-164

Industrial Liaison Office
ATTN: Susan Shansky
Monthly List of Publications
39-513

MIT Libraries
Collection Development
ATTN: MIT Reports
14E-210

B. Colby
PFC Library
NW16-255

EXTERNAL MAILINGS

International

Professor M.H. Brennan
Willis Plasma Physics Dept.
School of Physics
University of Sydney
N.S.W. 2006, Australia

Division of Plasma Physics
Institute of Theoretical Physics
University of Innsbruck
A-6020 Innsbruck
Austria

c/o Physics Section
International Atomic Energy Agency
Wagramerstrasse 5
P.O. Box 100
A-1400 Vienna, Austria

Laboratoire de Physique des Plasmas
c/o H.W.H. Van Andel
Dept. de Physique
Universite de Montreal
C.P. 6128
Montreal, Que H3C 3J7
Canada

Plasma Physics Laboratory
Dept. of Physics
University of Saskatchewan
Saskatoon, Sask., Canada S7N OWO

The Library
Institute of Physics
Chinese Academy of Sciences
Beijing, China

Mrs. A. Wolff-Degives
Kernforschungsanlage Julich GmbH
Zentralbibliothek - Exchange Section
D-5170 Julich - Postfach 1913
Federal Republic of Germany

Preprint Library
Central Research Institute for Physics
H-1525 Budapest, P.O. Box 49
Hungary

Plasma Physics Dept.
Israel Atomic Energy Commission
Soreq Nuclear Research Center
Yavne 70600
Israel

The Librarian (Miss DePalo)
Associazione EURATOM - CNEN Fusione
C.P. 65-00044 Frascati (Rome)
Italy

Librarian
Research Information Center
Institute of Plasma Physics
Nagoya University
Nagoya, 464
Japan

Dr. A.J. Hazen
South African Atomic Energy Board
Private Bag X256
Pretoria 0001
South Africa

EXTERNAL MAILINGS

National

Argonne National Laboratory
Argonne, IL 60439
ATTN: Library Services Dept.

Battelle-Pacific Northwest Laboratory
P.O. Box 99
Richland, WA 99352
ATTN: Technical Information Center

Brookhaven National Laboratory
Upton, NY 11973
ATTN: Research Library

U.S. Dept. of Energy
Washington, D.C. 20545
ATTN: D.O.E. Library

Roger Derby
Oak Ridge National Lab.
ETF Design Center
Bldg. 9204-1
Oak Ridge, TN 37830

General Atomic Co.
P.O. Box 81608
San Diego, CA 92138
ATTN: Library

Lawrence Berkeley Laboratory
1 Cyclotron Rd.
Berkeley, CA 94720
ATTN: Library

Lawrence Livermore Laboratory
UCLA
P.O. Box 808
Livermore, CA 94550

Oak Ridge National Laboratory
Fusion Energy Div. Library
Bldg. 9201-2, ms/5
P.O. Box "Y"
Oak Ridge, TN 37830

Dr. D. Overskei
General Atomic Co.
P.O. Box 81608
San Diego, CA 92138

Princeton Plasma Physics Laboratory
Princeton University
P.O. Box 451
Princeton, NJ 08540
ATTN: Library

Plasma Dynamics Laboratory
Jonsson Engineering Center
Rensselaer Polytechnic Institute
Troy, NY 12181
ATTN: Ms. R. Reep

University of Wisconsin
Nuclear Engineering Dept.
1500 Johnson Drive
Madison, WI 53706
ATTN: UV Fusion Library